Dielectronic recombination of boronlike argon

D. R. DeWitt, R. Schuch, H. Gao, W. Zong, S. Asp, and C. Biedermann
Department of Atomic Physics, Stockholm University, S-104 05 Stockholm, Sweden

M. H. Chen
Lawrence Livermore National Laboratory, P. O. Box 808, Livermore, California 94550

N. R. Badnell
Deptartment of Physics and Applied Physics, University of Strathclyde, Glasgow G40NG, Great Britain
(Received 25 August 1995)

We present measurements and calculations of $\Delta n=0$ dielectronic recombination resonances of boronlike argon between 0.2 and 6 eV. A storage ring equipped with an electron cooler was used for the measurements. Methods employed to reduce the electron energy distribution and improve the accuracy of resonance energy measurements have yielded an energy resolution of 30 meV full width at half maximum at low energies, and an energy uncertainty better than 30 meV. The high energy resolution results from the use of an adiabatic expansion technique to reduce the transverse electron energy distribution. The improved accuracy in energy determinations is achieved through the inclusion of variations in the ion velocity, which occur during scans of the electron velocity, in the relative velocity transformations. Calculations of the resonance strengths and energies were made using two different methods, multiconfiguration Dirac-Fock and multiconfiguration Breit-Pauli approximations. A comparison of the experimental data to the calculations shows fair agreement in both the spectral features and integrated intensities above 3 eV. However, poor agreement is found below 3 eV.

PACS number(s): 34.80.Kw, 34.80.Dp, 32.80.Hd

I. INTRODUCTION

Dielectronic recombination (DR) is an important electron-ion recombination process in laboratory and astrophysical plasmas [1–3]. This resonant process, which occurs in two steps, generally has an intensity much larger than the radiative recombination (RR) cross section in the same energy region, especially at higher energies. In the first step a free electron excites a bound electron by transferring an energy in excess of its kinetic energy; the free electron is thereby captured into a bound state. The second step in the vast majority of cases is the time-reversal process of autoionization, producing a net process of resonant elastic scattering. However, a small fraction (typically <0.001) decay by photon emission and a stable recombination product is formed. Theoretical treatment of the resonance cross sections involves calculation of the energies of doubly excited states as well as the calculation of autoionization and radiative decay rates, and experiments on DR provide a proving ground for these atomic structure calculations.

Within a little more than 12 years experiments have progressed from the first measurements of DR [4–6], to the present era of storage rings, which currently have an energy resolution of ~ 20 meV full width at half maximum at low energy, and perform measurements of highly-charged ions such as lithiumlike gold (Au^{76+}) [7]. In the high energy range ($E>500$ eV) electron beam ion traps are capable of performing measurements, including excitation and ionization as well as recombination, on highly charged ions at up to 200 keV [8,9].

Studies of DR have generally concentrated on few-electron targets. For example, hydrogenlike [10], heliumlike [11,12], and lithiumlike [13] systems have received a great deal of attention. While it might appear that a lithiumlike ion provides a complex target, at low and medium energies [below the core ($1s^2$) excitation threshold] this is essentially a one-electron target. At low energies that system is of special interest because of the fine-structure splitting of the ($\Delta n=0$) $2pn\ell J=\frac{1}{2}$ and $J=\frac{3}{2}$ series. In the present case, boronlike argon presents a genuine three-electron target at low energies. This complex target provides an enormous array of doubly excited states. Because the present studies involve $2s\rightarrow 2p$ excitation, complex fine-structure effects arise through the coupling of four electrons:

$$[1s^2\ J=0]2s^2(J=0);\ 2p(J=1/2)+e^- \rightarrow [1s^2 J=0]2s2p(J');\ 2p(J'');\ n\ell(J'''), \quad (1)$$

where J'' is the total angular momentum. A merged-beam technique has been used previously to measure the DR of boronlike N^{2+}, O^{3+}, and F^{4+} [14]. Agreement between theoretical and experimental determinations of dielectronic recombination energies and strengths has generally been good for few-electron systems, especially for $\Delta n=1$ resonances. The results of the present study show that this trend may not continue for more complex systems.

II. EXPERIMENT

A. Setup

The measurements were performed using the heavy ion storage ring CRYRING at Stockholm University's Manne Siegbahn Laboratory [15]. The $^{36}Ar^{13+}$ ions were supplied by an electron beam ion source, and boosted to the injection energy of 300 keV/amu by a radio frequency quadrupole

accelerator. Following injection the ions were accelerated to the highest circulation energy possible, approximately 11 MeV/amu, in order to reduce beam losses due to scattering and electron capture from residual gases. The ion beam lifetime at cooling was estimated to be 30 sec. The average number of ions in the ring was estimated to be 10^6 as determined from measurements of the ion beam current using an inductive current integrator [16]. The ion and electron beam currents were 1.7 μA and 158 mA, respectively.

As the ion velocity approaches that of the electrons in the cooler the ions experience a drag force that tends to equalize the average beam velocities. Over a period of approximately 2 sec the ion beam is cooled, and reaches a momentum spread $\Delta p/p < 10^{-5}$ as determined from the Schottky noise spectrum. More direct evidence of cooling is given by the reduction of the ion beam diameter, which contracts to approximately 1 mm; its initial diameter is roughly 2 cm. Overlap of the beams is assured, since the electron beam has a fixed diameter of 4 cm. The electron-ion interaction region, determined primarily by the deflection of the electron beam at the cooler's toroids, was estimated to be 80 ± 8 cm.

The measurements reported here take advantage of an order of magnitude reduction in the transverse temperature of the electron beam. The reduction is achieved through adiabatic expansion of the electron beam in the cooler's solenoidal field. Recent modifications to the cooler allow the magnetic field intensity near the cathode to be set to ten times the value used in the electron-ion interaction region. As the cyclotron orbit of the electrons expands in the decreasing magnetic field the transverse temperature is reduced to $T_\perp \rightarrow T_\perp B_{\rm cool}/B_{\rm cath}$, where $B_{\rm cool}$ is the magnetic field in the cooler's interaction region and $B_{\rm cath}$ is the magnetic field at the cathode. With this technique the transverse electron temperature is reduced from approximately $k_B T_\perp = 0.1$ eV (1100 K) at the cathode to $\simeq 10$ meV in the interaction region. In addition, the longitudinal electron energy distribution is further reduced by the kinematic transformation to the moving frame, and has an expected temperature of roughly 10^{-4} eV. Details may be found in Ref. [17].

Electron-ion recombination experiments using coolers as described here are essentially merged-beam experiments. Precise control over the range of interaction conditions is essential to the method. For the coaxial beam arrangement in storage rings, alignment of the two beams is virtually automatic, with fine tuning facilitated through optimization of the Schottky spectrum. In addition, reduction of the ion beam diameter limits interactions to the center of the electron beam, where space-charge-induced electric fields, as well as the resultant range of electron velocities, are minimal. Once the beams are aligned and cooled, interactions take place over a range of relative energies determined by the distribution of electron velocities and the difference, if any, in the average electron and ion velocities. Differences in the average velocities are achieved by altering the cathode voltage in a controlled manner; scans of relative interaction energies are performed using this method. Further details are given in Ref. [18].

After recombination in the cooler the charge-changed ions are separated from the primary beam as they pass through the 30° bending magnet located beyond the cooler. These separated Ar^{12+} ions are detected with a surface barrier detector (SBD) that has an efficiency of approximately 100%. Figure 1(a) shows the total number of detected Ar^{12+} ions as a function of time during the energy scans. This data contains four copies of the DR spectrum in the energy range 0–6 eV. Transformation of these data sets to center-of-mass energies is complicated by the variation of the average ion beam velocity during the energy scans. These four copies of the spectrum are used to fine tune the energy transformation, as described below.

B. Energy calculations

The cooling force between the electrons and ions is, nonrelativistically and without inclusion of magnetic effects arising from the weak solenoidal field which guides the electron beam, given by

$$\mathbf{F}(t) = F_0 c^2 \int L_c(\mathbf{v}_e, \mathbf{v}_i) f(\mathbf{v}_e) \frac{\mathbf{v}_e - \mathbf{v}_i}{|\mathbf{v}_e - \mathbf{v}_i|^3} d^3 v_e , \qquad (2)$$

where $F_0 = 4\pi Q^2 n_e r_e^2 m_e c^2$, Q is the ion charge, n_e is the electron density, r_e is the classical electron radius, $\mathbf{v}_i$ is the average ion velocity, $\mathbf{v}_e$ is the electron velocity, $f(\mathbf{v}_e)$ is the flattened electron velocity distribution

$$f(\mathbf{v}_e) = \frac{m_e}{2\pi k_B T_\perp} \left[\frac{m_e}{2\pi k_B T_\parallel} \right]^{1/2} \exp\left[- \frac{m_e v_\perp^2}{2 k_B T_\perp} \right] \times \exp\left[- \frac{m_e (v_\parallel - v_0)^2}{2 k_B T_\parallel} \right], \qquad (3)$$

and

$$L_c = \ln\left[\frac{|\langle \mathbf{v}_e \rangle - \mathbf{v}_i|}{Q r_e \omega_p} \frac{(\mathbf{v}_e - \mathbf{v}_i)^2}{c^2} \right] \qquad (4)$$

is the Coulomb logarithm. Here $\langle \mathbf{v}_e \rangle$ is the average electron velocity at a point in the scan, $v_0 = |\langle \mathbf{v}_e \rangle| - v_c$ is the detuning of the average electron velocity from its value at cooling v_c, and ω_p is the plasma frequency. The Coulomb logarithm as formulated here takes adiabatic screening of the ions into account [19]. During cooling, repeated collisions reduce the temperature of the ion beam. In that case any difference between the average beam velocities will damp out. During scans of the electron velocity, however, there is a tendency for the ions to accelerate to the electron velocity, with a drag force as described by Eq. (2). When the relative velocity is large, as in the case of high-energy DR resonances, the drag force is small and can be neglected. This can be understood by noting that the drag force scales as $\sim 1/\Delta v^2$ for large differences in average relative velocities Δv. Typically, for high-energy resonances, the scan begins with a sharp jump away from the ion (cooling) velocity to avoid prolonged interaction at small relative velocities.

When the range of interaction velocities includes the low-velocity region, acceleration of the ions occurs [20]. Since the interaction velocity is given by

$$\Delta v = (\langle v_e \rangle - v_i) \Big/ \left[1 - \frac{\langle v_e \rangle v_i}{c^2} \right], \qquad (5)$$

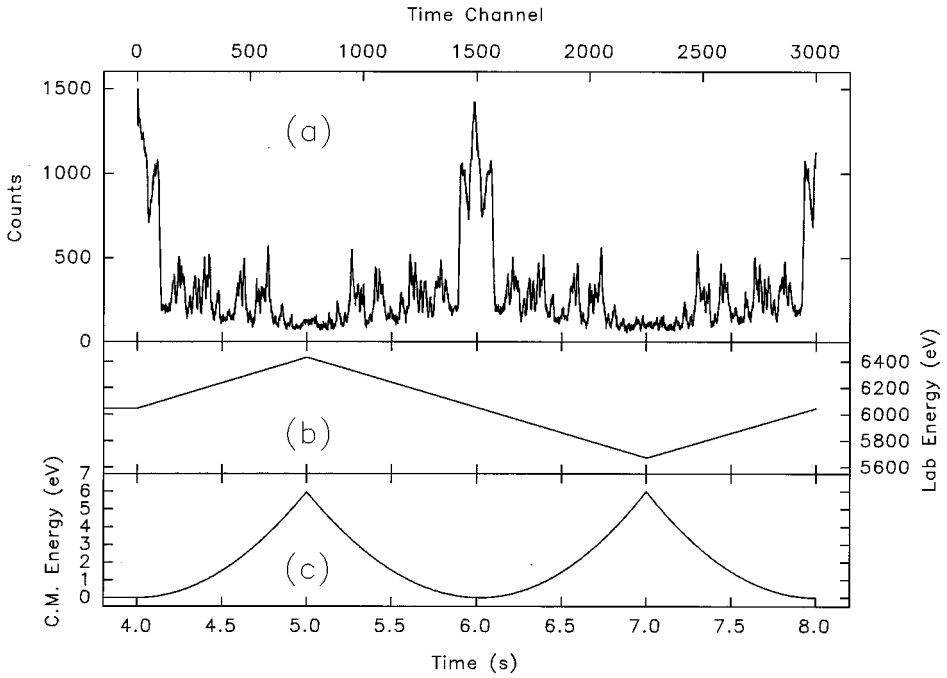

FIG. 1. (a) Four scans of the relative velocity were taken by ramping the electron velocity as shown in (b), producing the four data sets shown here. The sets merge at approximately 5.0, 6.0, and 7.0 sec. Sets two and four are mirror images of sets one and three. The scans follow 3 sec of cooling. These data were obtained in approximately 2 h during which 605 complete cycles took place. For reference, the interaction energies, uncorrected for electron space charge and ion acceleration, are shown in (c). Note the large structure appearing at the ends and center in (a). This large intensity is ten times the estimated radiative recombination rate at zero energy, and is produced by large DR resonances lying below 10 meV.

accurate determination of the ion velocity is essential. If the ion velocity varies during the scan of electron velocities, some estimate of average the ion velocity function $v_i(t)$ must be made. In the present case we approximated the ion velocity through the differential equation

$$\frac{dv_i}{dt}=\frac{\eta}{M_i}\frac{L_i}{L_r}F_z(t), \tag{6}$$

where M_i is the ion mass, L_i/L_r is the ratio of the interaction region to the length of the ring and represents the fraction of time over which the force is applied as ions circulate in the ring, $F_z(t)$ is the longitudinal component of the drag force, and η is a coupling parameter that will be described below. Equation (6) was solved numerically [21] using the estimated longitudinal electron velocity function $v_0(t)$ and the initial condition $v_i(0)=\langle v_e(0)\rangle$. The electron velocity function includes the effects of electron beam space-charge and distortion of the input ramp function by the cathode high voltage supply. As described in Ref. [18], accurate calculation of the space-charge requires an estimate of the trapped positive ion contribution. The trapped positive ions, formed by ionization of residual gases in the ring and bound by the electron beam space charge, increase the electron velocity in the cooler. Estimation of this space-charge compensation is made by comparing the electron velocity at cooling (as obtained from the Schottky frequency of the velocity matched ions) to the electron acceleration energy arising from the cathode voltage. The space-charge compensation ζ is then determined by the condition

$$eV_c-E_c=\left(\frac{1}{v_e}-\frac{\zeta}{v_c}\right)\frac{Ir_cm_ec^2}{e}\left[1+2\ \ln\left(\frac{r_t}{r_b}\right)-\left(\frac{r}{r_b}\right)^2\right], \tag{7}$$

where V_c and E_c are the cathode voltage and electron energy at cooling, respectively, v_e is the electron velocity, v_c is the electron velocity at cooling, I is the electron current, r_c is the classical electron radius, r_t and r_b are the radii of the cooler tube and electron beam, respectively, and r is the distance from the electron beam axis. For the evaluation of ζ at cooling $v_e=v_c$. The condition $r=0$ is assumed throughout the experiment. In order to test our estimation of the relative velocities determined from Eq. (6), data was acquired by scanning over the range of interest four times in a zig-zag pattern as shown in Fig. 1. The electron velocity was ramped to higher and then lower relative values, crossing the cooling velocity at the center of the ramping interval. In this way the drag force on the ion beam changed both strength and direction in a nontrivial manner. Our method consists of employing the numerical solution to Eq. (6) in Eq. (5) when calculating the interaction energies of the four data sets. The success of the method is gauged by the standard deviation obtained when comparing the four sets of energy values. Because the expression for the drag force, Eq. (2), is considered an approximation, we include a single adjustable parameter in the solution of Eq. (6). The parameter η is varied in order to minimize the standard deviation of the peak energies. Use of this parameter allows us to reduce the errors associated with uncertainties in the temperatures $T_\perp$, $T_\parallel$ and the length of the interaction region L_i. This parameter does not change the functional form of the drag force, and is thus interpreted as a coupling parameter.

Figure 2 shows the ion energy versus time as obtained from Eq. (6). The curve shown at the top illustrates the rapid acceleration of the ions at low relative velocities. In the neighborhood around $t=2$ sec the electron velocity passes through the original cooling velocity. At that point there is a rapid acceleration of the ions causing the relative velocities to cross zero before the electrons reach the cooling velocity. Immediately afterwards the ion velocity rapidly decreases as the electron velocity falls below the ion velocity. We have noticed that this curve is roughly symmetric when the drag force is weak, but asymmetric when the drag force is strong,

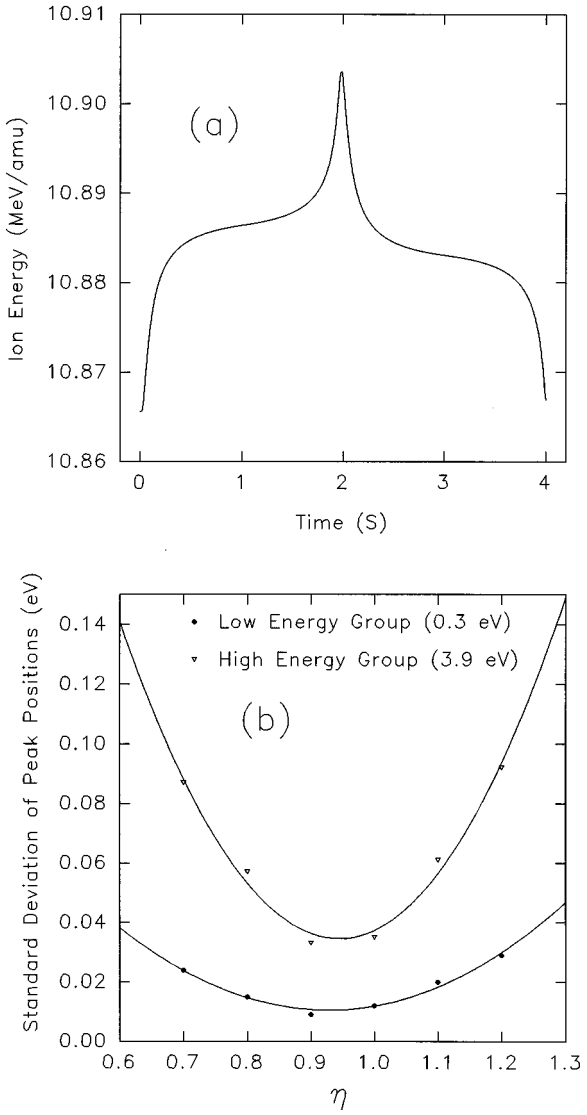

FIG. 2. (a) Ion energy as a function of time as calculated from the drag force. Note the sharp changes near zero relative velocity, at $t=0$, 2, and 4 sec. (b) Standard deviations of two peaks at opposite ends of the spectrum (see Fig. 3) as the drag force coupling parameter η is varied. The optimum value of η was taken as the value at the minimum of the quadratic fit curves shown.

with the plateau at $t<2$ sec appearing at higher energies than the $t>2$ sec plateau. The bottom curves show the standard deviations of two peaks selected to gauge the accuracy of the calculated ion energy. The first peak is located near 0.3 eV and the other near 3.9 eV (see Fig. 3). The coupling parameter η was varied and the data points shown in the figure obtained. Quadratic curves, also shown in the figure, were fit to these points to estimate the optimum value $\eta=0.935$. In practice this is an iterative process, since the drag force is strongly dependent on the electron temperatures used. Therefore the ion energy was calculated initially with expected values of these parameters, and preliminary fits to the DR peaks were made to determine the best-fit temperatures. The values used in the final drag force calculation were $k_BT_\perp=2\times10^{-2}$ eV and $k_BT_\parallel=1.5\times10^{-4}$ eV. When the initial estimates of these parameters, $k_BT_\perp=10^{-2}$ eV, $k_BT_\parallel=10^{-4}$ eV were used, the optimum value of η was

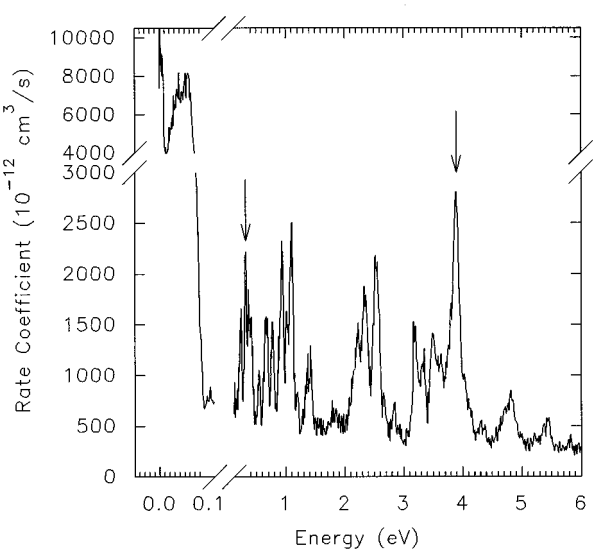

FIG. 3. Experimental results obtained from the first data set. These data have been corrected for dead time and beam decay, and the energies include the drag force correction as displayed in Fig. 2. The peaks at approximately 0.3 and 3.9 eV (arrows) were used to minimize the standard deviations of the four transformed energy values and therefore optimize the ion velocity correction. Fits of 48 lines were made to this and the other three sets of data. The nonresonant background above 0.2 eV is produced by RR and electron capture from residual gases. Below 0.2 eV the background is significantly enhanced beyond the calculated RR contribution; see Ref. [24].

estimated to be 0.75. We interpret the 0.935 value as further evidence that the temperatures obtained from the fits to the DR resonances are more accurate. The final standard deviations for lines fitted to the spectra above 0.2 eV are listed in Table I. As shown in Fig. 2, the peak near 0.3 eV has a standard deviation of less than 10 meV.

C. Data analysis

In order to determine resonance strengths from the spectra we converted the data to rate coefficients,

$$\alpha(E_c)=\frac{N_c'}{\delta t}\frac{\gamma^2}{n_eN_iL_i/L_r}, \tag{8}$$

where E_c is the energy calculated for channel c, N_c' is the corrected number of counts in channel c, δt (4/3000 sec) is the time interval per channel, γ is the Lorentz factor, n_e is the electron density at energy E_c, and N_i is the number of ions circulating in the ring.

In order to facilitate detailed off-line analysis, data was collected in event mode. Here an event is the detection of an ion by the SBD. Along with the SBD pulse height, the cathode voltage and time (relative to the start of the machine cycle) was recorded. The time is recorded because it is available at high precision directly in digital form, and is therefore immune to noise. Transformation of this time spectrum to cathode voltage is performed off-line by averaging, for each time channel, the recorded cathode voltages. In addition to a small correction for the decay of the ion beam during the

TABLE I. Experimental energies (eV) and strengths (10^{-20} cm^2 eV). The experimental energies have uncertainties that are dominated by systematic errors in the c.m. energy transformations; the standard deviation σ_E of the four values obtained from the fits is therefore listed. The corresponding strengths have uncertainties that, aside from any systematic errors, are determined from the standard error ϵ_s of the four fit values. The systematic uncertainty is 20%. The horizontal lines separate the energy regions as in Table II. Lines fit to the data below 0.2 eV are listed in Ref. [24].

E_{expt}	σ_E	S_{expt}	ϵ_s
0.235	0.009	60.9	12.8
0.257	0.008	90.0	14.8
0.331	0.009	179	6.55
0.364	0.020	57.9	8.50
0.389	0.013	86.1	10.4
0.422	0.012	78.4	1.65
0.452	0.012	70.1	3.90
0.562	0.012	45.5	1.85
0.660	0.012	61.4	2.64
0.700	0.013	98.9	3.54
0.796	0.013	106	1.50
0.908	0.013	59.7	3.10
0.957	0.014	145	5.10
1.031	0.014	84.9	2.55
1.092	0.013	97.7	7.20
1.128	0.013	132	8.40
1.204	0.016	26.8	0.64
1.379	0.019	43.2	1.22
1.451	0.019	54.3	0.55
1.862	0.024	19.6	2.33
2.152	0.024	31.2	3.24
2.235	0.026	83.8	5.70
2.325	0.031	80.1	5.80
2.393	0.024	103	9.85
2.516	0.028	84.2	8.15
2.577	0.026	115	4.81
2.665	0.032	37.5	4.12
2.853	0.028	14.9	1.90
3.218	0.021	8.58	1.93
3.344	0.021	66.8	0.74
3.516	0.021	87.6	0.59
3.630	0.020	63.9	1.24
3.739	0.017	54.7	3.83
3.827	0.019	88.8	2.63
3.915	0.025	183	3.12
4.007	0.030	53.5	1.74
4.102	0.026	28.4	0.95
4.346	0.019	13.1	1.74
4.684	0.033	20.0	3.06
4.791	0.038	29.3	3.86
4.878	0.034	25.9	6.30
5.324	0.046	5.96	0.04
5.439	0.030	17.7	0.30

scans, the number of counts N_c in each channel was corrected for dead time. In this case the dead time was dominated by the CAMAC-based data acquisition system and was approximately $T_d = 9 \times 10^{-4}$ sec. Thus the dead time was a substantial fraction of a channel width. Correction for the dead time was therefore nontrivial, since events in any channel have a large probability of blocking events in the following channel. Two methods were used to check our dead time corrections. First, the corrected rate at zero relative energy, near $t = 2$ sec in Fig. 1, was compared to the rate measured

with a fast counter gated to record at zero relative velocity; the corrected rate was approximately 9% lower. Any errors in the correction are expected to be smaller at the lower rates found elsewhere in the spectrum. Secondly, the dead time corrected rates were used to estimate, for each channel, the number of cycles in which exactly two events were expected to occur. This estimate was then compared to the actual number of cycles containing exactly two events as recorded in the list file. The agreement was found to be satisfactory except at the highest count rates, which occur near zero relative energy. This error is not unreasonable, since the event rates at this energy are high relative to the reciprocal dead time. The overall uncertainty is determined by possible systematic errors in the number of ions in the ring and the length of the interaction region. Each of these quantities has an uncertainty of 10%, so that the total systematic uncertainty is 20%. The final transformed spectrum from the first data set is displayed in Fig. 3.

D. Data fits

Although four sets of data were obtained from the scans, it is not practical to combine them through, for example, some sort of averaging. This is because the energies are not exactly matched, and combining them in that way would obscure the observed features. We therefore made independent fits to the four data sets, obtaining four sets of energies and resonance strengths. A total of 48 lines were fit to the experimental data. The criteria used in the fits were kept as simple as possible: we used the minimum number of lines necessary to reproduce the observed spectra. As discussed below, more than 200 resonances contribute to the spectra in this range. However, the number of meaningful features in the spectra is considerably less even at this energy resolution. As a result of this procedure, one-to-one correspondences between observed features, or the lines fit to them, are not attempted. This approach uses the number of lines fit to the data as one of the fit parameters. The transverse and longitudinal temperatures are the remaining essential parameters, and are common to all the fits to all four spectra. A local background, treated separately for each group of resonances, was included in the fits. A linear background was fit for energies greater than 0.5 eV. For the low-energy region, where the background is dominated by radiative recombination, the calculated radiative recombination rate coefficient, including screening [22], was used by employing an overall multiplicative constant as a fit parameter. As in the drag force calculation, an iterative procedure was used. The RR rate coefficient curve was calculated using the temperatures obtained from the initial fits [23], and an overall constant multiple of the calculated RR curve was used in the final fits. In the final fits the multiplicative RR constant was found to be 1.6. This might tend to indicate that a somewhat lower transverse temperature should have been used to calculate the RR curve. However, it should be noted that the nonresonant background is not a substantial feature in the low-energy region since the resonances in this region are strong and numerous. Therefore we do not interpret the background fit as a good measure of nonresonant recombination in this region. Indeed, the RR curve is used only to improve the accuracy of the fits to the DR resonances by providing the proper functional dependence to the background in this region. A detailed description of the treatment of the nonresonant background in these data can be found in Ref. [24].

Although the ideal procedure would allow both temperatures as free parameters along with the intensities and energies of the lines, we found that with such a large number of free parameters unreasonable values were obtained for the temperatures. We know, however, from several measurements that the longitudinal temperature is 0.15 meV/k_B or less. Since the width and shape of the spectrum in the low-energy range is dominated by the transverse temperature, along with the estimated number of resonances within a given feature, we fixed the longitudinal temperature to this value. Our procedure then rested on the condition that the transverse temperature used in the determination of intensities and energies be the same throughout the energy range for all four data sets. Preliminary fits were made to the group of resonances near 0.3 eV to determine the transverse temperature. The value obtained from this procedure was $k_B T_\perp = 20 \pm 2$ meV. The transverse temperature was expected to be close to 10 meV as discussed previously. The reason for the higher observed temperature is not clear. The group of resonances near 0.3 eV was chosen because the density of calculated resonances in this region is fairly low, and the large central peak in this group may contain a single resolved resonance, allowing us to determine the approximate line shape. This spectral feature therefore has a large influence on the estimated temperatures obtained from the fits. Given the overlap of the observed features overall, values obtained for these parameters are influenced by the number of lines assumed to contribute to the shape of any given spectral feature, so that the appearance of any well separated line is of importance. The natural linewidths were not used in the fits.

Results from the fits to the four sets of data above 0.2 eV are listed in Table I. As mentioned previously, the fit lines either cannot be identified with specific resonances or represent an aggregate of resonances in the immediate vicinity. No estimate of the variation in the cathode voltage ramp from cycle to cycle is included in the fit model; however, it cannot be concluded that the widths do not include an instrumental component. It is anticipated that as transverse temperatures decrease through future improvements in cooler design, resonances near zero energy will require increasing attention to instrumental effects. With these points in mind, we can only say that the true temperatures of the electron beam have upper bounds given by the fit results.

The four sets of line energies and strengths were averaged to obtain the values reported in the table. The energies were determined by minimizing the standard deviation of peaks at opposite ends of the spectrum. Thus, the reported uncertainties σ_E are standard deviations of the corresponding energy values. This reflects the fact that these uncertainties are model dependent, or nonstatistical in nature. The average values of the resonance strengths, however, are not model dependent, aside from any systematic errors resulting from the dead time corrections or errors in other parameters such as the interaction length or the number of ions in the ring; that is, they are statistical in nature. Thus, the reported uncertainties in these quantities are standard errors, $\epsilon_s = \sigma/\sqrt{N}$ where σ is the standard deviation and $N(=4)$ is the number of observations.

III. THEORY

A. General

In the isolated resonance approximation (in which no interference between close lying resonances is included), and with no interference between the direct and resonance recombination processes, the energy–averaged DR cross section from an initial state i to a final state f via an intermediate doubly excited state d is given in atomic units by [25]

$$\bar{\sigma}_{\mathrm{DR}}(idf)=\frac{\pi^2}{\Delta E E_d}\frac{g_d}{2g_i}A_a(d\rightarrow i)\omega_d, \tag{9}$$

with

$$\omega_d=\frac{A_r(d\rightarrow f)}{\Sigma_j A_a(d\rightarrow j)+\Sigma_k A_r(d\rightarrow k)}. \tag{10}$$

Here, g_d and g_i are the statistical weight factors for the intermediate and initial states, respectively; E_d is the Auger energy and ΔE is the energy bin.

In general, the spectrum of DR cross sections is quite complex and small changes in theoretical resonance positions can give rise to markedly different looking results on comparison with experiment; the total integrated DR cross section changes little of course. It is often necessary to adjust the theoretical resonance positions. However, spectroscopic observations of autoionizing levels are, by their nature, relatively sparse and ''fitting'' to the DR measurements that we are trying to analyze is a rather circular approach.

B. Multiconfiguration Dirac-Fock method

In the present work the Auger and radiative transition rates were calculated from first-order perturbation theory using the multiconfiguration Dirac-Fock (MCDF) atomic model [26,27]. In the MCDF model the energy levels and bound-state wave functions were calculated in the extended-average-level scheme [26]. The calculations were carried out in intermediate coupling with configuration interaction from the same complex. All possible Auger channels and electric dipole transitions leading to stabilized bound states were taken into account in the evaluations of radiative branching ratios.

In general, the resonances below 6 eV arise from transitions of the form $2s2p^2n\ell$ ($n=6,7$) with $2s-2p_{1/2}$ excitation and $2s2p^2n\ell$ ($n=9,10$) with $2s$-$2p_{3/2}$ excitation. The calculations indicate that transitions to $n=8$ do not appear in this energy range.

In the MCDF calculations the $2s$-$2p$ excitation energies for boronlike argon were found to differ from experiment [28] by amounts ranging from 0.3 to 1.6 eV. As a result, the calculated rate coefficients agreed rather poorly with the experimental results. After correcting the resonance energies using the experimental $2s$-$2p$ excitation energies fair agreement between MCDF theory and experiment has been attained. The remaining discrepancies are probably due to errors in the calculated resonance energies. It will be a challenge for the theorists to calculate the resonance energies to better than 0.05 eV for such complex systems with so many DR lines.

C. Multiconfiguration Breit-Pauli method

The intermediate coupling calculations, using the Breit-Pauli Hamiltonian (hereafter referred to as MCBP), were carried out within the independent processes and isolated resonance approximations [29] using the AUTOSTRUCTURE computer code [30]. The following Ar^{13+} configurations were included: $2s^22p$, $2s2p^2$, and $2p^3$. Continuum and Rydberg electron orbitals were subsequently coupled to each of the preceding configurations and all possible configuration-mixed autoionization and electric-dipole radiation transition probabilities were calculated. In addition, radiative stabilizing transitions of the form $2s2p^2n\ell\rightarrow 2s2p^2n'\ell'$ were included hydrogenically for $n'>2$ and explicit configuration mixed for $n'=2$. The dominant recombination resonances over 0–5 eV are of the form $2s2p^2\,{}^2S,{}^2P,{}^2Dn\ell$ for $n=5,6,7$ with small contributions from $2s2p^2\,{}^4Pn\ell$ for $n=10,11$; the $n=9$ are just closed. The contribution from $2s^22p(J=3/2)n\ell$ for $n=30-60$ is extremely small (stabilization is via the high-n Rydberg electron) and cannot be distinguished in the experiment.

In order to adjust the theoretical energies, we assume that the resonance positions, relative to the ground level i of the initial ion, are given by $E_j-E_i+E_{n\ell}$. Here E_j is an excited-level energy of the initial ion and $E_{n\ell}=-z^2/\nu_\ell^2$, where z is the residual charge of the initial ion and the quantum defect is $\nu_\ell=n-\delta_\ell$. The calculated E_j-E_i for the resonances are replaced by spectroscopic values for Ar^{13+} [28]. We note that only a small number of nonautoionizing level energies are required by this approach.

IV. RESULTS AND DISCUSSION

The data analysis procedure described above yielded four sets of fit results, each containing 48 fit lines. The mean energies and strengths of the 43 lines above 0.2 eV are given in Table I. Results for the data below 0.2 eV include a strong enhancement of the nonresonant background that cannot be accounted for by radiative recombination, making interpretation of the intensity very close to zero relative energy dependent on assumptions regarding the nonresonant background. Those fit results and their analysis have been published separately [24]. According to the calculations, the doubly excited states in the spectrum below 6 eV contain outer electrons in orbitals with $n\leqslant 11$. In this experiment the n-level cutoff due to field ionization in the bending magnet was estimated to be 40 [31], well above the range of active n levels contributing to the observed spectrum.

In order to compare the experimental results with theory we convoluted the averages of the four DR strengths obtained from the fits to produce a single curve that describes the experimental results. This curve is shown at the top of Fig. 4. We consider this procedure to be superior to a simple averaging of the four data sets, or the accumulation of all the data in a single energy scan, for two primary reasons. First, the nontrivial transformations of the four data sets to the c.m. frame provides a mechanism for fine tuning the transformation parameters, since without the constraint of self-consistency imposed on the energy correction model there would be no objective method of testing the corrections. In such a case one could argue that there is no greater value in the corrected energies than in the uncorrected energies. Sec-

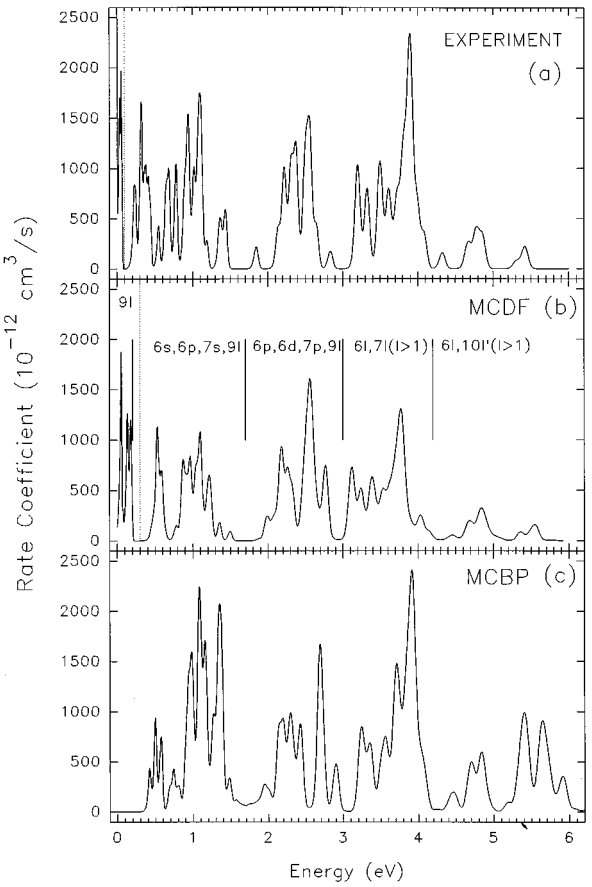

FIG. 4. (a) Convolution of average line strengths obtained from fits to the four sets of experimental data; see Table I. The lines have been convoluted with the temperatures obtained from the fits, $k_BT_\perp = 20$ meV, $k_BT_\parallel = 0.15$ meV. The curve on the left of the dotted line has been multiplied by 1/4. (b) Convolved resonances from MCDF theory. The data to the left of the dotted line have been multiplied by 1/2. The vertical lines divide the energy regions according to the dominant configuration of the outer electron orbital as in Table II. (c) Convolved resonances from MCBP theory.

ond, this method provides error bars for both the energies and intensities of the fit lines. Because least-squares fitting is inherently immune to overall intensity variations, the reported error bars are a somewhat more realistic gauge of the random variations of the intensities. To these advantages one can also add that comparison of the total intensities in the four sets provides a check on the decay of the ion beam during the scan. This is valuable because the decay of the ion beam is not given by the same exponential lifetime measured for the cooled beam, since the strong nonresonant recombination contribution to ion loss is switched off during the scans. In this regard we note that the scanning period is limited by the ion beam lifetime, the synchrotron injection-acceleration interval and the cooling period. As mentioned previously the systematic uncertainty in the intensities is 20%.

The MCDF calculated resonances for this system are shown in Fig. 4(b). The 242 calculated cross sections have been convoluted with the same electron energy distribution used to convolute the experimental fit lines. The Lorentz width of each resonance was used in the convolution, since 75 of the lines have widths greater than 5 meV. In fact, one of the calculated lines, a $2s2p^26f\ ^3G_5$ resonance at 4.71 eV, has a width of 62.3 meV. The agreement is qualitatively good. Comparison of the two curves shows that the most strikingly similar features occur between approximately 3 and 4 eV. According to the calculations the intensity between 3 and 4 eV arises from $2s2p^2n\ell$ states with $n=6,7$ and $\ell \geq 2$. However, we note that these assignments are approximations, since the same outer electron configuration may produce resonances at energies outside these designated ranges according to their parentage (i.e., the coupling of the core $^2S,^2P,^2D$). Table II lists electron configurations and integrated cross sections for five broad energy regions. The experimental cross sections below 0.2 eV overlap with the rising nonresonant recombination peak in this range, and their contribution to the overall rate of recombination depends on the model assumed for the nonresonant background. There are indications that the nonresonant background at low energies may be strongly enhanced beyond the RR contribution, therefore the value listed in Table II is a lower bound on the DR strength in this region. From the table one can see that the experimental intensities are twice those of MCDF theory between 0.2 and 1.7 eV, but only 17% higher overall between 1.7 and 6.0 eV.

The MCBP calculated cross sections are shown in Fig. 4(c). The energy averaged cross sections, binned in 20 meV intervals, were folded with the same electron distribution used for the experimental and MCDF curves. Table II includes the total integrated cross sections. No resonances appear in the region below 0.2 eV; however, the total integrated cross section between 0.2 and 4.2 eV differs from experiment by only 1%. The rather large feature in the calculated spectrum just below 6 eV is probably larger than the experimen-

TABLE II. Integrated cross sections I (10^{-20} cm^2 eV). The configurations have the form $2s2p^2n\ell$; the resonances contained in each interval are listed according to the dominant outer electron orbitals from the MCDF calculation.

$n\ell(a)$	$E_{\rm low}(eV)$	$E_{\rm high}(eV)$	$I_{\rm expt}$	$I_{\rm theory}$ MCDF	MCBP
9ℓ	0.0	0.2	>5178 [a]	1581.2	—
$6s,6p,7s,9\ell$	0.2	1.7	1578	769.53	1493.88
$6p,6d,7p,9\ell$	1.7	3.0	569.3	582.54	629.47
$6\ell,7\ell$ $(\ell \geq 2)$	3.0	4.2	712.5	507.00	773.80
$6\ell,10\ell'$ $(\ell \geq 2)$	4.2	6.0	111.96	98.52	460.01

[a]This value depends on the assumed form of the nonresonant background at low energies; see Ref. [24].

tal result because a decay channel is calculated to be just open, when in fact it is just closed. The two broadest resonances found are the $2s2p^2 6f\ ^3G_J$ for $J=4$ and 5 at 4.69 and 4.72 eV with widths of 68.2 and 70.3 meV, respectively. However, we found that very little difference resulted from convoluting the Lorentzian as opposed to energy-averaged DR cross sections.

No recombination into metastable ($2s^2 2p\ ^2P_{3/2}$) targets was observed. This metastable state has a calculated lifetime of 10 ms and an excitation energy of 2.8 eV. Such a short lifetime precludes the survival of such targets after the 4-sec injection-cooling interval. Although we are not aware of any calculations of the cross sections for excitation of this state through collisions with the rest gas, the fraction of ions in this state is expected to be negligible. For comparison, the combined contributions to ion beam loss (ionization, capture, and scattering involving residual gases, and intense recombination with cooling electrons) during cooling cause the beam to decay with a half-life of approximately 20 sec. It is possible to excite this metastable through electron impact when scanning the energy range above 2.8 eV. However, a simple estimate indicates that an electron impact excitation (EIE) cross section of approximately $\sigma^{\mathrm{EIE}} \simeq 10^{-16}\ \mathrm{cm}^2$ would produce an equilibrium metastable population of only 10%. Given the weak oscillator strength for the metastable transition such a large cross section is not realistic.

Data were also obtained in the 140–190 eV energy region for the measurement of $\Delta n=1$ resonances for the present system. The results of that work are presented in Ref. [32].

V. CONCLUSION

Experimental and theoretical results for the dielectronic recombination of Ar^{13+} in the few eV range have been presented. We have found fair quantitative agreement between theoretical and experimental spectral features and intensities in the energy range above 3 eV. However, the calculations do not reproduce the spectral features below 3 eV, and have mixed results for the integrated intensities. The discrepancies are probably due to errors in the calculated doubly excited state energy levels in this region. Comparison of the experimental and theoretical spectra indicates that this complex multielectron system requires further study. In particular, we have found in the present case that at high resolution the qualitative description of the experimental spectrum is hampered by the need for theoretical energies accurate to roughly 20 meV. Anticipated improvements to the electron cooler at CRYRING and other storage rings should soon bring the transverse electron temperature down to the 1-meV range, further improving the experimental resolution at low energies [33].

ACKNOWLEDGMENTS

The authors would like to thank the staff and technicians of CRYRING and those of the electron beam ion source (CRYSIS) for their assistance in this experiment. The experimental work at CRYRING was supported by the Swedish Natural Science Research Council (NFR) and the Knut and Alice Wallenberg Foundation. The work of M.H.C. was performed under the auspices of the U. S. Department of Energy by the Lawrence Livermore National Laboratory under Contract No. W-7405-ENG-48. The work of N.R.B. was supported in part by the U. K. EPSRC under Contract No. GR/K/14346 with the University of Strathclyde.

[1] A. Burgess, Astrophys. J. **139**, 776 (1964).
[2] M. J. Seaton and P. J. Storey, in *Atomic Processes and Applications*, edited by P. G. Burke and B. L. Moisewitsch (North-Holland, Amsterdam, 1976).
[3] J. Dubau and S. Volonte, Rep. Prog. Phys. **43**, 199 (1980).
[4] J. B. A. Mitchell, C. T. Ng, J. L. Forand, D. P. Levac, R. E. Mitchell, A. Sen, D. B. Miko, and J. Wm. McGowan, Phys. Rev. Lett. **50**, 335 (1983).
[5] D. S. Belić, G. H. Dunn, T. J. Morgan, D. W. Mueller, and C. Timmer, Phys. Rev. Lett. **50**, 339 (1983).
[6] P. F. Dittner, S. Datz, P. D. Miller, C. D. Moak, P. H. Stelson, C. Bottcher, W. B. Dress, G. D. Alton, N. Nešković, and C. M. Fou, Phys. Rev. Lett. **51**, 31 (1983).
[7] W. Spies *et al.*, Phys. Rev. Lett. **69**, 2768 (1992).
[8] P. Beiersdorfer, T. W. Phillips, K. L. Wong, R. E. Marrs, and D. A. Vogel, Phys. Rev. A **46**, 3812 (1992).
[9] R. E. Marrs, S. R. Elliott, and D. A. Knapp, Phys. Rev. Lett. **72**, 4082 (1994).
[10] D. R. DeWitt, D. Schneider, M. W. Clark, M. H. Chen, and D. Church, Phys. Rev. A **44**, 7185 (1991).
[11] R. Ali, C. P. Bhalla, C. L. Cocke, and M. Stockli, Phys. Rev. Lett. **64**, 633 (1990).
[12] L. H. Andersen, G-Y. Pan, H. T. Schmidt, N. R. Badnell, and M. S. Pindzola, Phys. Rev. A **45**, 7868 (1992).
[13] G. Kilgus, D. Habs, D. Schwalm, A. Wolf, N. R. Badnell, and A. Müller, Phys. Rev. A **46**, 5730 (1992).
[14] P. F. Dittner, S. Datz, R. Hippler, H. F. Krause, P. D. Miller, P. L. Pepmiller, C. M. Fou, Y. Hahn, and I. Nasser, Phys. Rev. A **38**, 2762 (1988).
[15] K. Abrahamsson, G. Andler, L. Bagge, E. Beebe, P. Carlé, H. Danared, S. Egnell, K. Ehrnstén, M. Engström, C. J. Herrlander, J. Hilke, J. Jeansson, A. Källberg, S. Leontein, L. Liljeby, A. Nilsson, A. Paal, K.-G. Rensfelt, U. Rosengård, A. Simonsson, A. Soltan, J. Starker, and M. af Ugglas, Nucl. Instrum. Methods Phys. Res. Sect. B **79**, 269 (1993).
[16] K. B. Unser, Report No. CERN SL/91-42 (BI), 1991 (unpublished).
[17] H. Danared, G. Andler, L. Bagge, C. J. Herrlander, J. Hilke, J. Jeansson, A. Källberg, A. Nilsson, A. Paál, K.-G. Rensfelt, U. Rosengård, J. Starker, and M. af Ugglas, Phys. Rev. Lett. **72**, 3775 (1994).
[18] D. R. DeWitt, R. Schuch, T. Quinteros, H. Gao, W. Zong, H. Danared, M. Pajek, and N. R. Badnell, Phys. Rev. A **50**, 1257 (1994).

[19] H. Poth, Phys. Rep. **196**, 135 (1990).
[20] However, an induction accelerator has been developed for TSR, which damps ion acceleration during detuning. See Ch. Ellert, D. Habs, E. Jaeschke, T. Kambara, M. Music, D. Schwalm, P. Sigray, and A. Wolf, Nucl. Instrum. Methods Phys. Res. Sect. A **314**, 399 (1992).
[21] Our algorithm is based on the Bulirsch-Stoer routines of W. H. Press, S. A. Teukolsky, W. T. Vetterling, and B. P. Flannery, *Numerical Recipes in C*, 2nd ed. (Cambridge University Press, Cambridge, 1992), p. 724.
[22] Daniel J. McLaughlin and Yukap Hahn, Phys. Rev. A **43**, 1313 (1991).
[23] Lars. H. Andersen and Jakob Bolko, Phys. Rev. A **42**, 1184 (1990).
[24] H. Gao, D. R. DeWitt, R. Schuch, W. Zong, S. Asp, and M. Pajek, Phys. Rev. Lett. **75**, 4381 (1995).
[25] K. LaGattuta and Y. Hahn, Phys. Rev. A **24**, 2273 (1981).
[26] I. P. Grant, B. J. McKenzie, P. H. Norrington, D. F. Mayers, and N. C. Pyper, Comput. Phys. Commun. **21**, 207 (1980).
[27] M. H. Chen, Phys. Rev. A **31**, 1449 (1985).
[28] R. L. Kelly, J. Phys. Chem. Ref. Data, Suppl. 1 **16**, 408 (1987).
[29] M. S. Pindzola, N. R. Badnell, and D. C. Griffin, Phys. Rev. A **46**, 5725 (1992).
[30] N. R. Badnell, J. Phys. B **29**, 3827 (1986).
[31] C. Bottcher, D. C. Griffin, and M. S. Pindzola, Phys. Rev. A **34**, 860 (1986).
[32] W. Zong, D. R. DeWitt, R. Schuch, H. Gao, S. Asp, and E. Justiniano (unpublished).
[33] H. Danared (private communication).